LAWRENCE
LIVERMORE
NATIONAL
LABORATORY

UCRL-PROC-218150

Electrical Conductivity Calculations from the Purgatorio Code

S. B. Hansen, W. A. Isaacs, P. A. Sterne, B. G. Wilson, V. Sonnad, D. A. Young

January 13, 2006

NEDPC-2005
livermore, CA, United States
October 17, 2005 through October 21, 2005

Electrical Conductivity Calculations from the Purgatorio Code (U)

S.B. Hansen, W.A. Isaacs, P.A. Sterne, B.G. Wilson, V. Sonnad, and D.A. Young

Lawrence Livermore National Laboratory, Livermore, California, 94550

*The Purgatorio code [Wilson et al., JQSRT **99**, 658-679 (2006)] is a new implementation of the Inferno model describing a spherically symmetric average atom embedded in a uniform plasma. Bound and continuum electrons are treated using a fully relativistic quantum mechanical description, giving the electron-thermal contribution to the equation of state (EOS). The free-electron density of states can also be used to calculate scattering cross sections for electron transport. Using the extended Ziman formulation, electrical conductivities are then obtained by convolving these transport cross sections with externally-imposed ion-ion structure factors. (U)*

Introduction

Accurate modeling of astrophysical and laboratory plasmas requires accurate equation of state (EOS) data for a variety of elements over a wide range of material conditions, from the solid state to the rare plasma and high energy-density regimes. However, precise EOS measurements exist only for a restricted set of materials at select temperature-density points. Equation of state models which give reliable data, constrained by experiments, for any element at any set of conditions are needed to fill in the gaps between data points.

Equation of state models typically consist of three parts, including descriptions of the electron-thermal and ion contributions to the EOS and a semi-empirical fit stitching these two contributions to the cold curve. The Purgatorio code [1] is a recent implementation of David Liberman's Inferno model [2], which belongs to a family of historically successful ion-in-cell or neutral-pseudo-atom (NPA) approaches to the electron-thermal contribution to the equation of state [see, for example, Refs. 3-5].

Purgatorio numerically solves the Dirac equation for the major and minor components of the bound wave functions normalized to unity over all space, with analytic forms employed outside of the Wigner-Seitz cell radius R_{ion} where $V(r) = 0$. Continuum wave functions are computed on an adaptive energy grid to resolve detailed

information on the density of states. Matching the numerical wave functions to analytic forms at $R_{\rm ion}$ gives phase shifts $\delta_\kappa(\varepsilon)$, which are used in conductivity calculations. The energy grid, initially logarithmic, is refined to capture resonances which form in the continuum when bound states are destroyed by pressure ionization. Capturing the resonances is essential for the self-consistent calculation and is ensured either by the refinement described in [1] or by tracking changes in the phase shifts.

The bound and continuum electron densities are determined by populating the wave functions according to their statistical weights, modulated by the Fermi distribution function $f(\varepsilon,\mu) = (1+e^{(\varepsilon-\mu)/\tau})^{-1}$, with the chemical potential μ varied to ensure neutrality:

$$\int_0^{R_{ion}} 4\pi r^2 \rho_{\rm tot}(r)\mathrm{d}r = Z$$

with

$$\rho_{\rm tot}(r) = \rho_{\rm bound}(r) + \rho_{\rm continuum}(r)$$

$$4\pi r^2 \rho_{\rm bound}(r) = \sum_i f(\varepsilon_i,\mu) 2|\kappa_i| \left\{P_i^2(r) + Q_i^2(r)\right\}$$

$$4\pi r^2 \rho_{\rm continuum}(r) = \int_0^\infty \mathrm{d}\varepsilon\, f(\varepsilon,\mu) \sum_\kappa 2|\kappa| \left\{P_{\kappa,\varepsilon}^2(r) + Q_{\kappa,\varepsilon}^2(r)\right\}$$

The potential is determined from the total electron density and iterated to self-consistency using Local Density Approximations (LDA) to the exchange and correlation potentials [6].

Converged values of the electron density and its bound and continuum components are given in Fig. 1(a) for Ni at solid density and a temperature of 1 eV. The bound electrons have a clear shell structure, as labeled on the figure, which is absent in the Thomas-Fermi fluid description (gray lines). The continuum electron distribution, which in the Thomas-Fermi approximation would be a smooth increasing function of r, shows a pronounced feature associated with the unbound 3*d* state. Figure 1(b) shows the density-of state like quantity $X(\varepsilon)$ for this case, where the bound states are represented by delta functions at their negative-energy eigenvalues and the continuum $X(\varepsilon)$ is given by

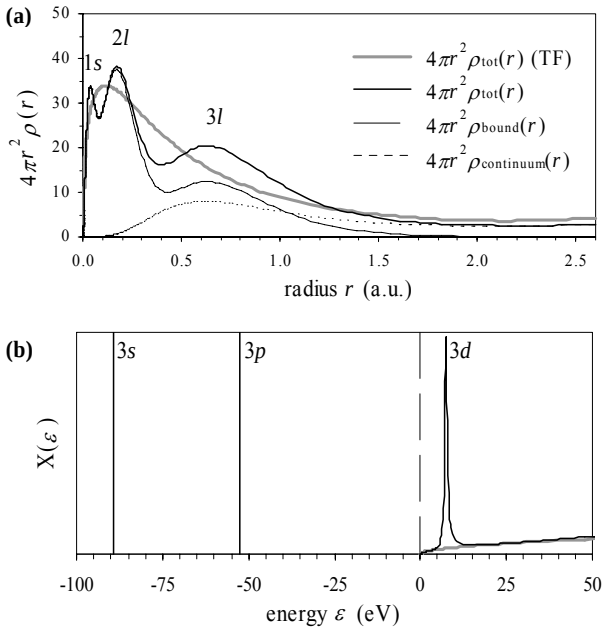

Fig. 1. Calculations for Ni at 1 eV and solid density (8.91 g/cm^3). (a) Electron distributions within the Wigner-Seitz cell (R_{ion} = 2.60 a.u.). The gray line is the distribution in the Thomas-Fermi approximation. (b) Bound state energy eigenvalues ($\varepsilon < 0$) and continuum $X(\varepsilon)$ ($\varepsilon > 0$), which exhibits a resonance feature corresponding to the pressure-ionized 3*d* orbital. The gray line is $X^{\rm ideal}(\varepsilon)$.

$$X(\varepsilon) = \sum_\kappa 2|\kappa| \int_0^{R_{\rm ion}} \mathrm{d}r \left\{P_{\kappa,\varepsilon}^2(r) + Q_{\kappa,\varepsilon}^2(r)\right\}$$

In solid-density nickel, the 3*d* state is pressure ionized and appears as a resonance in the continuum, causing a significant deviation from the equivalent quantity for free waves $X^{\text{ideal}}(\varepsilon) = p(1+\alpha^2\varepsilon)/(\pi^2 n)$.

A non-relativistic sister code to Purgatorio, which gives results very close to those of Purgatorio for low-*Z* ions, has also been developed [7] and used to test variations in the model. Its results are used in some of the figures in this paper.

In subsequent sections, we will describe a recent implementation of the extended Ziman formulation for electrical conductivity. A fairly extensive range of experimental conductivity data exists which can be compared with the Purgatorio conductivity calculations and used to guide the development of the model parameters, particularly the definition of the average ion charge. We show some of these comparisons and give a discussion of their consequences along with conclusions and our plans for future work.

EOS data

The accurate treatment of continuum electrons and the stringent numerical tolerances in Purgatorio permit the extraction of thermodynamic quantities, such as pressure and entropy, through numerical differentiation of the internal energy. Prototypical results from Purgatorio, including the principal Hugoniots of Be and Al and pressure vs. energy isochors for low-density Al, have been published recently [1].

We focus in this section on the ion charge. Unlike other thermodynamic quantities, which have a unique thermodynamically consistent definition, the average ion charge can be computed in several ways. The most straightforward of these is to define the ion charge to be the total number of continuum electrons:

$$Z_{\text{continuum}} = \int_0^{R_{ion}} 4\pi r^2 \rho_{\text{continuum}}(r)\mathrm{d}r = \int_0^{\infty} f(\varepsilon,\mu) X(\varepsilon)\mathrm{d}\varepsilon$$

This definition includes both the electrons in the ideal density of states, which have wave functions distributed throughout the material, and the "quasi-bound" electrons in the resonance features, whose wave functions have extensive tails but are fairly localized about the ion center (see Fig. 1). An alternative definition counts only the free electrons in the ideal density of states, excluding the population of quasi-bound or resonant states:

$$Z_{\text{free}} = \int_0^{\infty} f(\varepsilon,\mu) X^{\text{ideal}}(\varepsilon)\mathrm{d}\varepsilon$$

Finally, we can define the free electrons to be those on the surface of the ion sphere:

$$Z_{\text{WS}} = 4\pi R_{ion}^2 \rho_{\text{tot}}(R_{ion})/n$$

This definition largely excludes electrons in continuum resonances but can include a portion of any negative-energy bound states that "leak out" of the ion sphere. The electrons on the surface of the ion sphere are free to move between ions and can thus be considered extensive.

In most cases, Z_{WS} and Z_{free} are close to each other, and all three values tend to converge at high temperature and low density. However, at densities high enough to pressure ionize valence orbitals and temperatures low enough to significantly populate resonance states, the three quantities can differ widely: for example, in the case shown in Fig. 1, $Z_{\text{continuum}} = 10$, $Z_{\text{WS}} = 2.36$, and $Z_{\text{free}} = 1.78$.

A comparison of the three definitions of the free electron density with experimental data obtained from x-ray scattering of Be targets [8] is given in Fig. 2. The low-temperature points agree best with $Z_{continuum}$, while the high temperature point agrees with the calculations excluding continuum resonances. Similar trends are seen in comparisons of Purgatorio calculations with carbon data [9]. The given figure is similar to Fig. 6 of Ref. 5, which shows SCAALP calculations that fall very near the Purgatorio $Z_{continuum}$ values, along with ACTEX [4] and NPA [3] calculations which follow the experimental data fairly closely across the given temperature range.

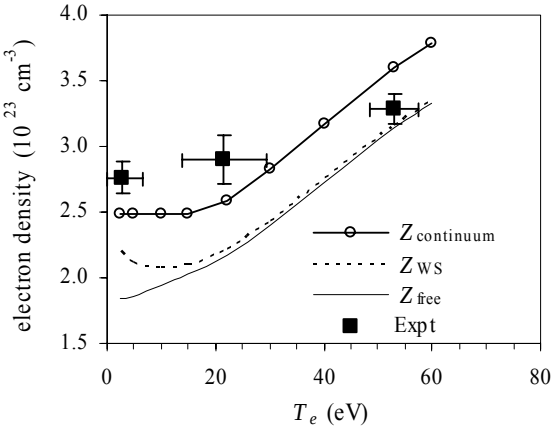

Fig. 2. Comparison of the electron density in 1.85 g/cm^3 Be as measured by x-ray scattering [8] with three different formulations of the calculated average ion charge, as described in the text.

Electrical conductivity

A recent addition to the Purgatorio code is the calculation of static (direct-current) electrical conductivities. The approach follows the work of Rinker [10, 11] in its implementation of the extended Ziman formulation [12] and is informed by the works of Perrot and Dharma-Wardana [*e.g.* 3, 13, 14], Yuan, Sun, and Zheng [15], Blancard and Faussurier [5], and Johnson [16].

The extended Ziman formulation for the electrical resistivity of liquid metals is based on linear response theory, where free electrons in a metal are uniformly accelerated until they collide with an ion and are scattered. The expression for the resistivity takes on a Drude-like form:

$$\eta = \frac{1}{nZ_i}\left(\frac{1}{\tau}\right)$$

where nZ_i is the charge carrier density and τ is a relaxation time (time between scattering events). The relaxation time depends on the scattering cross section $\sigma(\varepsilon)$ and the velocity distribution of the free electrons:

$$\left(\frac{1}{\tau}\right) = -\frac{1}{3\pi Z_0}\int_0^\infty \sigma(\varepsilon)\frac{\partial f(\varepsilon,\mu)}{\partial \varepsilon}\mathrm{d}\varepsilon$$

According to Rinker, the quantity Z_0 is constrained on variational grounds to be identical to Z_{free} when the Boltzmann equation is valid [10], although there is no similar constraint on the number of charge carriers Z_i.

In the *t*-matrix formulation of Evans *et al*, the total scattering cross section $\sigma(\varepsilon)$ is obtained by integrating the angle-dependent differential cross section $d\sigma(p,\theta)/d\theta$ over all possible scattering angles θ:

$$\sigma(\varepsilon) = \int_0^{2p} q^3\left(\frac{d\sigma(p,\theta)}{d\theta}\right)S(q)dq$$

$$\frac{d\sigma(p,\theta)}{d\theta} = \frac{1}{p^2}\left\{\left|\sum_\kappa |\kappa| e^{i\delta_\kappa(p)} \sin[\delta_\kappa(p)] P_l(\cos\theta)\right|^2 + \left|\sum_\kappa \frac{|\kappa|}{i\kappa} e^{i\delta_\kappa(p)} \sin[\delta_\kappa(p)] P_l^1(\cos\theta)\right|^2\right\}$$

where ($l = \kappa$ for $\kappa > 0$ and $-\kappa-1$ for $\kappa \le 0$), $P_l(\cos\theta)$ and $P_l^1(\cos\theta)$ are the Legendre and associated Legendre polynomials, respectively, the relativistic dispersion relation $p^2 = \varepsilon(2 + \varepsilon\alpha^2)$ is assumed, and the integration is performed over the momentum transfer vector $q^2 = 2p^2[1-\cos\theta]$. The phase shifts $\delta_\kappa(\varepsilon)$ are calculated by matching the analytic wave functions for $r > R_{\text{ion}}$ to the numerical wave functions inside the ion cell (see [15 and 16]). The integration over q is modulated by the structure factor $S(q)$, which is the Fourier transform of the ion-ion pair correlation function and which will be discussed in some detail below.

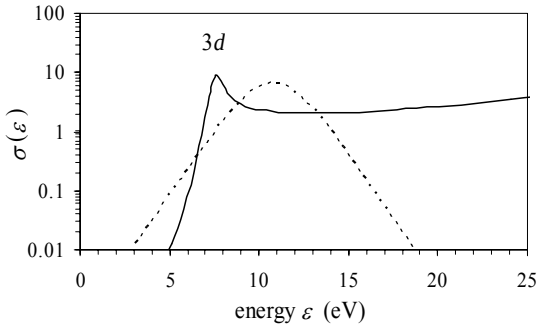

Fig. 3. Scattering cross section (solid line) and $-\partial f(\mu,\varepsilon)/\partial\varepsilon$ (dashed line) for solid-density Ni at 1 eV.

Figure 3 shows the scattering cross section for solid density Ni at a temperature of 1 eV, along with the derivative of the Fermi function. Both quantities appear in the integral for the resistivity. The 3*d* resonance, which was prominent in the continuum density of states (see Fig. 1) is also clearly evident in the scattering cross section. Indeed, the density-of-states-like quantity $X(\varepsilon)$ given above in terms of $P_{\varepsilon,\kappa}(r)$ and $Q_{\varepsilon,\kappa}(r)$ can also be expressed in terms of the phase shifts:

$$X(\varepsilon) = X^{\text{ideal}}(\varepsilon) + \sum_\kappa 2|\kappa| \frac{d\delta_\kappa(\varepsilon)}{d\varepsilon}$$

Resistivity calculations have a multifaceted dependence on the structure of the electron distribution in the average atom: there is a direct dependence on the number of charge carriers Z_i; a fairly straightforward dependence on the average velocity of the free electrons (and thus the chemical potential μ) through the Fermi distribution function; and a strong dependence on the single-ion scattering cross section, which is directly related to the density of states and any associated resonance or band structure. In addition, the resistivity depends on the ionic structure of the plasma through the ion structure factor $S(q)$. The electronic contributions can be isolated in weakly coupled plasmas at moderate to high temperatures and low densities, where the structure factor approaches unity at the dominant q values and its exact functional form has little impact on the calculations.

Calculated resistivities for Al and Ni are given in Fig. 4 along with experimental values obtained by DeSilva and Katsouros in wire vaporization experiments [17]. The solid lines show the calculations using $Z_i = Z_{\text{free}}$ and the dashed lines show the results using $Z_i = Z_{\text{continuum}}$. At the lowest densities, the two values are nearly equal and the calculated resistivities agree well with the data. But as the density increases, valence bound states are pressure-ionized, leading to resonance structure in the continuum and large differences between the two definitions for the average ion charge. The effect is

larger for Ni, with its 3*d* resonance and ten valence electrons, than for Al, with its *3p* resonance.

From Fig. 4, it appears that the calculations using $Z_i = Z_{continuum}$ do a better job of describing the nonmetal to metal transition, which occurs in the experimental data near 0.1 g/cm^3 for Al and 0.3 g/cm^3 for Ni. However, using $Z_i = Z_{continuum}$ introduces into the resistivity the rather sharp changes caused by pressure ionization with increasing density, while the experimental data does not bear any indication of shell structure. The selection $Z_i = Z_{continuum}$ also does not universally improve agreement with experiment, particularly for calculations of resistivity near melt (although in such cases we are far from the weak coupling limit and the dependence is complicated by the structure factor). So far, we have produced results using $Z_i = Z_{free}$, retaining as charge carriers only those electrons which are truly free and excluding those which have a high probability of being localized. Rinker has noted that this choice can provide an upper limit on the resistivity [11]; a firm limit on a smoothly varying quantity may be more useful for model development than a jagged intermediate quantity.

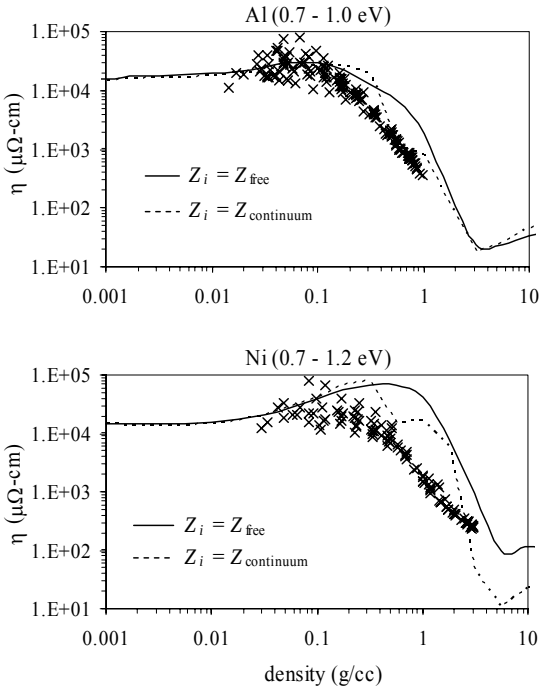

Fig. 4. Calculated electrical resistivities at 0.86 eV as a function of material density for Al and Ni, showing the effect of different selections for the number of charge carriers Z_i. The data points are from experiments by DeSilva and Katsouros [17] at the indicated temperature ranges.

The structure factor *S*(*q*)

The differential cross section $d\sigma(p,\theta)/d\theta$ is valid only for a single ion. To describe scattering within an extended medium, we require the structure factor $S(q)$. The quantity $[S(q)-1]$ is the Fourier transform of the ion pair correlation function $g(r)$, which gives the probability of encountering an ion at a given radius. A number of researchers have obtained consistent structure factors in liquid metals using interatomic potentials derived from the electronic structure in average atom or neutral pseudo-atom models [*e.g.* 3, 14, 18]. We have found that the exact shape of the structure factor is not of critical importance, even in the solid state limit (see below), and seek instead an approximation to the structure factor that preserves the broad observed dependence of resistivity with temperature.

The strong and weak coupling limits of ions in an extended medium are conveniently delineated by the ion-ion coupling parameter $\Gamma_{ii} = Z_i^2/(\tau R_{ion})$, with τ the ion temperature in atomic units. (It seems clear that for this parameter the appropriate choice

for Z_i is Z_{free}, since electrons in the localized quasi-bound states effectively shield ions from one another.)

In weakly coupled plasmas with $\Gamma_{ii} < 1$, the thermal energy of the ions is much smaller than their potential energy. As the temperature decreases or the density increases, short-range order begins to occur in the plasma, Γ_{ii} increases, and something like a liquid state develops. Continuing these trends leads to crystallization. For the one-component plasma (OCP), melting occurs at $\Gamma_{ii} \sim 172$, so that any material with a Γ_{ii} larger than this value can be considered a crystalline solid. In the strongly coupled (quantum) limit, the ion pair correlation function $g(r)$ consists of sharp peaks at crystal lattice sites; its transform $S(q)$ is also sharply peaked.

These qualitative comments are illustrated in Fig. 5, which shows structure factors for $\Gamma_{ii} = 10$, 172, and 1000. The solid lines for the $\Gamma_{ii} = 10$ and 172 cases were calculated using the fit to the OCP $S(q)$ given by Young, Corey, and DeWitt [19]. The solid line for $\Gamma_{ii} = 1000$ was calculated using the Fourier transform of a $g(r)$ composed of thermally broadened Gaussian peaks at the spherically averaged lattice sites of a fcc crystal. The dashed lines are the simple Debye-Hückel structure factors $S(q) = (qr_d)^2/[1 + (qr_d)^2]$ with the Debye radius $r_d = \sqrt{R_{ion}^3 \tau/(3Z_i^2)}$ which are valid at high temperatures. In 1968, Mermin determined that Debye-Hückel gives a lower limit for $S(q)$ at any temperature [20]. The gray lines in Fig. 5 are the inelastic components of the solid-state structure factor as described by Baiko *et al*. in Refs. 21and 22 and are discussed further below.

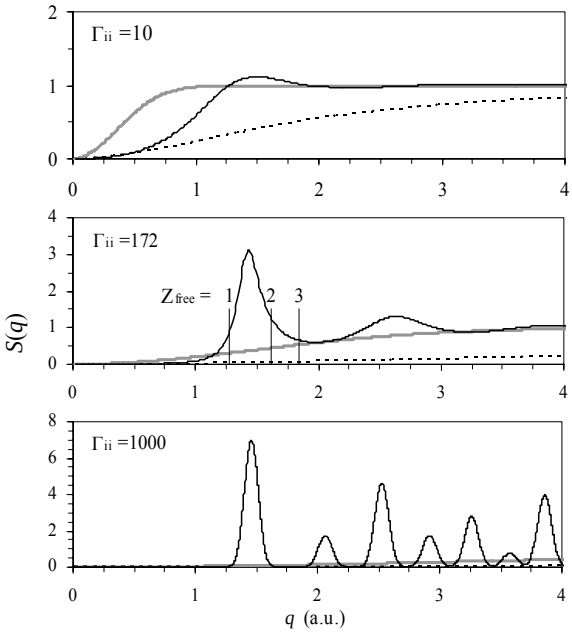

Fig. 5. Various structure factors $S(q)$ as a function of the ion-ion coupling parameter Γ_{ii}. Solid lines are OCP $S(q)$ for $\Gamma_{ii} = 10$ and 172 and fcc for $\Gamma_{ii} = 1000$. Gray lines are the inelastic components of the solid-state $S(q)$ given by [21, 22] continued into the liquid phase. Dashed lines are Debye-Hückel. The vertical lines on the center plot indicate $q = 2p_F$, the momentum cutoff for integration, for various ion charges.

We have indicated on the $\Gamma_{ii} = 172$ curve in Fig. 5 the locations of the value $q = 2p_F$ for various values of Z_{free}. In the zero-temperature limit, the Fermi momentum $p_F = (3\pi^2 n Z_{free})^{1/3}$ fixes the upper limit of the electron velocity distribution. The integral of the differential cross section modulated by the structure factor in resistivity calculations is carried out to at least $2p_F$. This has important consequences for the temperature dependence of the calculated resistivity: for metals with more than one valence electron, the integral over the structure factor always includes at least the first

peak of $S(q)$, regardless of the temperature. In fact, as the temperature decreases and the Bragg peaks narrow, the integral may capture a larger share of $S(q)$. Since the electronic structure reaches a low-temperature limit beyond which the differential cross section and the values Z_{free} and $Z_{continuum}$ are constant, the effect of the changing structure factor tends to increase the resistivity or leave it unchanged with decreasing temperature in the solid-state limit. But this is not at all what is experimentally observed: the resistivity of most solid metals decreases with temperature due to a reduction in phonon scattering at low temperatures.

In an application to fully ionized but highly degenerate plasmas, Baiko *et al*. propose that only the inelastic component of the structure factor should be included in resistivity calculations, since the elastic components, which correspond to the sharp peaks in the structure factor, translate but do not scatter the free electrons [21, 22]. We have implemented their prescription for the solid state $S(q)$ in our calculations, both with and without their recommended cutoff at the equivalent radius of the Brillouin zone (they set $S(q) = 0$ for $q < q_B = (6\pi^2 n)^{1/3}$. For the liquid phase, Baiko *et al*. use the OCP $S(q)$ but subtract out the elastic components representing short-range order in the liquid. We have implemented both this option and the option of continuing their inelastic $S(q)$ for the solid state into the liquid phase.

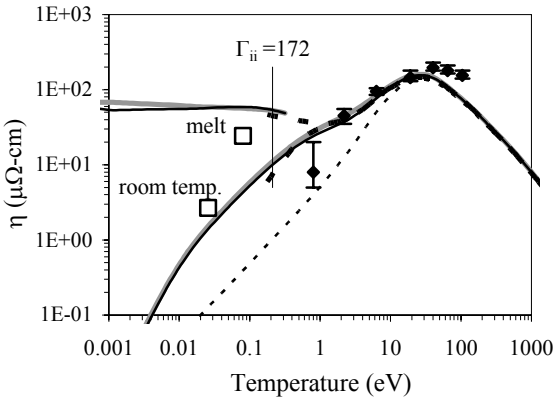

Fig. 6. Resistivity of solid-density aluminum as a function of temperature with various $S(q)$. The thin dashed line uses the Debye-Hückel $S(q)$. The other lines split into two branches at low temperatures. In the upper branch, fcc (black), bcc (gray) and OCP (bold dashed) $S(q)$ are used. In the lower branch, only the inelastic portions of the bcc (black excluding $q < q_B$ and gray including all q) and OCP (bold dashed) $S(q)$ are used. Data points at room temperature and melt are given along with laser-plasma data from [23]

Figure 6 illustrates the temperature dependence of the resistivity for solid density Al calculated using various formulations of $S(q)$. Experimental points are given for Al at room temperature and melt, as well as for higher temperatures as measured by Milchberg [23]. At high temperatures, there is very little dependence on $S(q)$ and the calculated resistivities agree rather well with the laser plasma data. At temperatures below 10 eV, calculations with different $S(q)$ diverge. The low-temperature limit for Z_{free} in solid-density Al is 2, giving an upper limit for the integration over $S(q)$ of $2p_F = 1.61$. At low temperatures, calculations using either the bcc or fcc $S(q)$ sample the first elastic scattering peak (see Fig. 5) and thus remain constant or slightly increase with decreasing temperature, deviating strongly from the room temperature measurements. The behavior of the calculation using only the inelastic portion of the bcc $S(q)$ [21, 22] conforms much better to our expectation in the solid state. Calculations using the Debye-Hückel $S(q)$ appear to offer a reliable minimum value for the resistivity.

Conclusions

We have described the code Purgatorio, a new implementation of the Inferno model with a highly accurate treatment of continuum wave functions and stringent numerical tolerances. Purgatorio can provide the electron-thermal component of equation of state data for use in hydrodynamic modeling, including electrical conductivity data. The ability to calculate conductivity opens up a wide range of experimental data for comparison which can help to define ambiguous quantities such as the average ion charge and refine the model parameters, in particular the exchange and correlation potentials. Investigations into improvements to the LDA treatment of exchange and correlation potentials are ongoing.

Acknowledgements

We thank Hugh DeWitt and Dima Yakovlev for valuable assistance with our investigations into the low-temperature structure factor. We are also grateful to Alan DeSilva of the University of Maryland for providing resistivity data. This work was performed under the auspices of the U.S. Department of Energy by the University of California Lawrence Livermore National Laboratory under contract No. W-7405-Eng-48.

References

[1] B. Wilson, V. Sonnad, P. Sterne, and W. Isaacs, "PURGATORIO—a new implementation of the INFERNO algorithm," *Journal of Quantitative Spectroscopy and Radiative Transfer* **99**, 658-679 (2006).

[2] D.A. Liberman, "Self-consistent field model for condensed matter," *Phys. Rev. B* **20**, 4981-4989 (1979).

[3] F. Perrot, "Dense simple plasmas as high-temperature liquid simple metals," *Phys. Rev. A* **42**, 4871–4883 (1990) and F. Perrot, "Ion-ion interaction and equation of state of a dense plasma: Application to beryllium," *Phys. Rev. E* **47**, 570-582 (1993).

[4] F.J. Rogers and D.A. Young, "Validation of the activity expansion method with ultrahigh pressure shock equations of state," *Phys. Rev. E* **56**, 5876-5883 (1997).

[5] C. Blancard and G. Faussurier, "Equation of state and transport coefficients for dense plasmas," *Phys. Rev. E* **69**, 016409 1-15 (2004).

[6] L. Hedin and B.I. Lundqvist, "Explicit local exchange-correlation potentials," *J. Phys. C* **4**, 2064-83 (1971).

[7] S.B. Hansen *et al*., "Temperature determination using $K\alpha$ spectra from *M*-shell Ti ions," *Phys. Rev. E* **72**, 036408 1-15 (2005).

[8] S.H. Glenzer, G. Gregori, R.W. Lee, F.J. Rogers, S.W. Pollaine, and O.L. Landen, "Demonstration of Spectrally Resolved X-Ray Scattering in Dense Plasmas," *Phys. Rev. Lett.* **90**, 175002 1-4 (2003).

[9] G. Gregori, S.H. Glenzer, K.M. Campbell *et al*., "X-ray Scattering measurements of radiative heating and cooling dynamics," submitted 2006.

[10] G.A. Rinker, "Electrical conductivity of a strongly coupled plasma," *Phys. Rev. B* **31**, 4207 (1985).

[11] G.A. Rinker, "Systematic calculations of plasma transport coefficients for the Periodic Table," *Phys. Rev. A* **37**, 1284 (1988).
[12] R. Evans, B.L. Gyorffy, N. Szabo, and J.M. Ziman, in *The Properties of Liquid Metals*, edited by S. Takeuchi (Wiley, New York, 1973).
[13] F. Perrot and M.W.C. Dharma-wardana, "Electrical resistivity of hot dense plasmas," *Phys. Rev. A* **36**, 238–246 (1987).
[14] F. Perrot and M.W.C. Dharma-wardana, "Theoretical issues in the calculation of the electrical conductivity," *International Journal of Thermophysics* **20**, 1299 (1999).
[15] J.K. Yuan, Y.S. Sun, and S.T. Zheng, "Calculation of the electrical conductivity of strongly coupled plasmas," *Phys. Rev. E* **53**, 1059-1067 (1996).
[16] W.R. Johnson et al., "Kubo-Greenwood Theory for an Average Atom," unpublished, 2004.
[17] A.W. DeSilva and J.D. Katsouros, "Electrical conductivity of dense copper and aluminum plasmas,"*Phys. Rev. E* **57** 5945-5951 (1998); *ibid*. **59**, 3774 (1999); Ni data from private communication.
[18] G. Faussurier, "Description of strongly coupled Yukawa fluids using the variational modified hypernetted chain approach," *Phys. Rev. E* **69**, 066402 1-23 (2004).
[19] D.A. Young, E.M. McCorey, and H.E. DeWitt, "Analytic fit to the one-component-plasma structure factor," *Phys. Rev. A* **44**, 6508 (1991).
[20] N.D. Mermin, "Exact Lower Bounds for Some Equilibrium Properties of a Classical One-Component Plasma," *Phys. Rev*. **171**, 272-275 (1968).
[21] D.A. Baiko, A.D. Kaminker, A.Y. Potekhin, and D.G. Yakovlev, "Ion Structure Factors and Electron Transport in Dense Coulomb Plasmas," *Phys. Rev. Lett*. **81**, 5556-5559 (1998).
[22] A.Y. Potekhin, D.A. Baiko, P. Haensel, and D.G. Yakovlev, "Transport properties of degenerate electrons in neutron star envelopes and white dwarf cores," *Astronomy and Astrophysics* **346**, 345-353 (1999).
[23] H.M. Milchberg, R.R. Freeman, S.C. Davey, and R.M. More, "Resistivity of a Simple Metal from Room Temperature to 10^6 K," *Phys. Rev. Lett*. **61**, 2364-2367 (1988).